Towards Nuclear Physics as Precision Science

Ulf-G. Meißner

Helmholtz-Institut für Strahlen- und Kernphysik and Bethe Center for Theoretical Physics, Universität Bonn, D-53115 Bonn, Germany
Institute for Advanced Simulation and Institut für Kernphysik, Forschungszentrum Jülich, D-52425 Jülich, Germany
Tbilisi State University, 0186 Tbilisi, Georgia

Abstract

I discuss the foundations of Nuclear Lattice Effective Field Theory and discuss a number of applications to nuclear structure and reactions, including α-α scattering, clustering in nuclei and the first steps towards calculations beyond next-to-next-to-leading order.

Keywords: *Effective field theory, nuclear forces, lattice, Monte Carlo methods*

1 Introduction: The big picture

Nuclear physics is an important part of the Standard Model (SM) of the strong, electromagnetic and weak interactions. While only about 5% of the energy-matter content of the Universe is a visible matter, this mostly comes in the form of atomic nuclei and is the stuff we are made off. In a way, the precise understanding of the formation of strongly interacting composites in forms of hadrons and nuclei can be seen as the last frontier of the SM. Furthermore, precision calculations in nuclear physics may open the door to unravel physics beyond the SM, e. g., through the electric dipole moments of light nuclei or neutrinoless $\beta\beta$-decay. Last but not least, as the generation of elements in the Big Bang and in stars exhibits some fine-tunings, the variation of the fundamental constants of the SM gives access to the multiverse and thus allows to investigate the anthropic view of the Universe.

Nuclear Lattice Effective Field Theory (NLEFT) combines the successful description of the forces between two, three and four nucleons in the continuum (see Evgeny Epelbaum's contribution to these Proceedings [1]), as initiated by Weinberg [2, 3], with stochastic methods to numerically exactly solve the nuclear A-body problems. NLEFT also allows to perform *ab initio* studies of nuclear reactions. This is an important feature as nuclear structure and reactions should be considered together. In the following, I will briefly outline some basic ingredients and a number of results obtained in this framework. More recent developments will be given in Dean Lee's contribution to these Proceedings [4].

Proceedings of the International Conference 'Nuclear Theory in the Supercomputing Era — 2018' (NTSE-2018), Daejeon, South Korea, October 29 – November 2, 2018, eds. A. M. Shirokov and A. I. Mazur. Pacific National University, Khabarovsk, Russia, 2019, p. 28.

http://www.ntse.khb.ru/files/uploads/2018/proceedings/Meissner.pdf.

2 Basics of nuclear lattice simulations

Nuclear lattice simulations or NLEFT is a new method to investigate the nuclear few- and many-body problem. In this approach, the Euclidean space-time is represented by a discrete hyper-cubic volume, $V = L \times L \times L \times L_t$, with the spatial (temporal) length L (L_t) and corresponding lattice spacings a and a_t, respectively. The nucleons are considered as the basic constituents and are placed on the lattice sites, see a schematic pictorial in the left panel of Fig. 1. The interactions between the nucleons are given by the same chiral EFT potentials as in the continuum, for a review see, e. g., Ref. [5] simply adapted to the lattice formulation, see, e. g., Ref. [6]. The Coulomb interaction between the protons can also straightforwardly be included [7]. The chiral NN interactions obey a power counting, where the leading order (LO) consists of the static one-pion exchange and two four-nucleon contact terms. At higher orders, two-pion exchange, corrections to the one-pion exchange as well as contact interactions with an even number of derivatives appear. The latter are accompanied by low-energy constants (LECs) that must be fitted to the nucleon-nucleon scattering data. At the next-to-next-to-leading order (N2LO), the three-nucleon forces appear that contain two new LECs, that must be fitted to a three-nucleon system or three-nucleon scattering data. On the lattice, the finite lattice spacing entails an UV cut-off, as the maximal momentum is given by $p_{\max} = \pi/a$. For the most commonly used value of the lattice spacing, $a \simeq 2\,\mathrm{fm}$, one has $p_{\max} = 314\,\mathrm{MeV}$, which corresponds to a very soft interaction. Monte Carlo (MC) methods can then be used to numerically exactly solve the A-body problem for a given set of NN and NNN interactions. A very important ingredient in these simulations is the approximate Wigner SU(4) symmetry of the nuclear interactions, that is crucial in suppressing the malicious sign oscillations that plague fermion MC studies at finite baryonic density [8, 9]. The remaining sign oscillations are caused by SU(4) non-symmetric contact terms as well as by the one-pion-exchange. For more details, see the review [10] and the upcoming textbook [11].

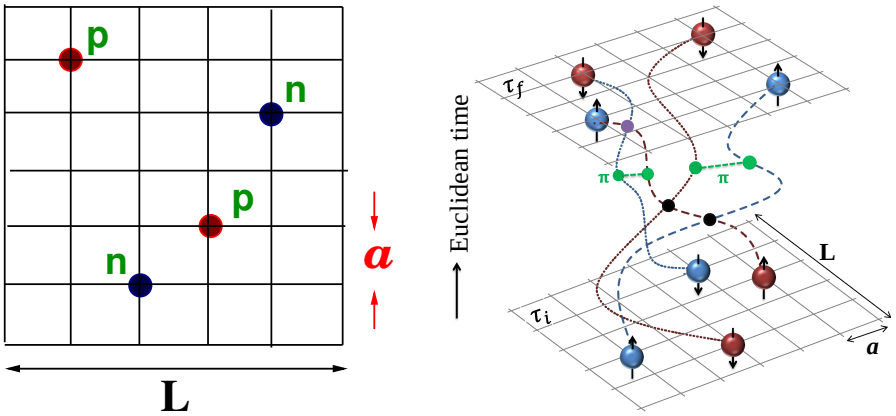

Figure 1: Left panel: Neutrons and protons on a space-time lattice with spatial length L and lattice spacing a. Right panel: Evolution of a ^{4}He nucleus in Euclidean time.

The central object of NLEFT is the A-nucleon correlation function,

$$Z_A(t) = \langle \Psi_A | \exp(-tH) | \Psi_A \rangle, \tag{1}$$

with t being the Euclidean time and Ψ_A being a Slater determinant of A free nucleons or a more sophisticated correlated initial/final state. From the transient energy

$$E_A(t) = -\frac{d}{dt} \ln Z_A(t) \tag{2}$$

one can infer the ground state energy of the A-nucleon system via

$$E_A^0 = \lim_{t\to\infty} E_A(t). \tag{3}$$

Similarly, the expectation value of any normal-ordered operator follows from

$$Z_A^{\mathcal{O}} = \langle \Psi_A | \exp(-tH/2)\, \mathcal{O}\, \exp(-tH/2)\, | \Psi_A \rangle \tag{4}$$

in the limit of infinite Euclidean time,

$$\lim_{t\to\infty} (Z_A^{\mathcal{O}}(t)/Z_A(t)) = \langle \Psi_A | \mathcal{O} | \Psi_A \rangle. \tag{5}$$

Excited state properties can also be extracted. In order to compute the low-lying excited states of a given nucleus, the Euclidean time projection method is generalized to a multi-channel calculation [12]. The Euclidean time evolution of a ^{4}He nucleus is depicted in the right panel of Fig. 1. Initial states are either properly antisymmetrized free standing waves of four particles or more complex correlated configurations. With the help of auxiliary fields, the multi-nucleon interactions and the pion exchanges can be mapped onto insertions on a single nucleon world-line, which makes such a computation most accessible for parallel computing. One major advantage of this approach is that all possible configurations are sampled, in particular also four nucleons, on one lattice site. This already lets one suspect that clustering will emerge naturally in this approach.

3 Results from nuclear lattice simulations

3.1 General remarks

Before discussing results obtained using NLEFT, a few general remarks are in order. As already stressed, nuclear structure and reactions dynamics should be treated on the same footing. This has important implications for the simulations. While originally all LECs have been determined in few-nucleon systems, which has led to a number of intriguing results, it was realized later that nucleus-nucleus collisions should also be used for determining some LECs as this appears to be advantageous in pinning down more precisely the three- and higher-body forces. Furthermore, the framework of nuclear lattice simulations could only be established as a novel quantum many-body method since one was able to solve problems that before could not be mastered in the well established schemes based on the same chiral forces.

Most results in NLEFT have been obtained with an NNLO action that involves a Gaussian smearing of the two LO contact interactions, with the smearing parameter

fixed from the average S-wave np effective range. The canonical lattice had a coarse lattice spacing of $a = 1.97\,\mathrm{fm}$ and $L \simeq 10 \ldots 16\,\mathrm{fm}$ depending on the nucleus or system under investigation. For such a coarse lattice, the NLO and NNLO corrections can be treated as perturbations, in particular, the contribution from the two-pion exchange can be absorbed in the LECs of the $4N$ operators. At this order, one has 11 LECs related to np, nn and pp scattering as well as two $3N$ LECs. The $2N$ LECs were determined from fits to the np phase shifts using the spherical wall method [13] and its refinement [14] as well as to the nn and pp scattering lengths. The $3N$ LECs were determined from a fit to the triton binding energy and the spin-doublet neutron-deuteron scattering phase shift. The first non-trivial prediction is then the ^{3}He–^{3}H binding energy difference [7,15] which comes out as 0.78(5) MeV close to the empirical value of 0.76 MeV. Ground state energies up to ^{28}Si can now be calculated with a few percent accuracy and an error of about 1%, see Refs. [16, 17]. Note, however, that at this order there is still some residual lattice spacing dependence when a is varied between 1 and 2 fm, see Refs. [18, 19]. An effective four-nucleon operator has been utilized to overcome this effect. This residual lattice spacing dependence, however, disappears at NNNLO as than the np phase shifts are independent on a for a varying between 1 and 2 fm within uncertainties as recently shown in Ref. [20].

Excited states can be computed with a comparable accuracy. In Fig. 2, the LO calculation of the first two 0^+ states in ^{12}C is shown, starting from various initial states (plane waves and alpha cluster states) [21]. One set of these initial states directly gives the ground state (left panel), whereas the other set first traces out the first excitation with the same quantum numbers as shown by the intermediate plateau (right panel). This is the famous Hoyle state [22]. The thermalization of various initial states with growing Euclidean time to almost the same energy gives a

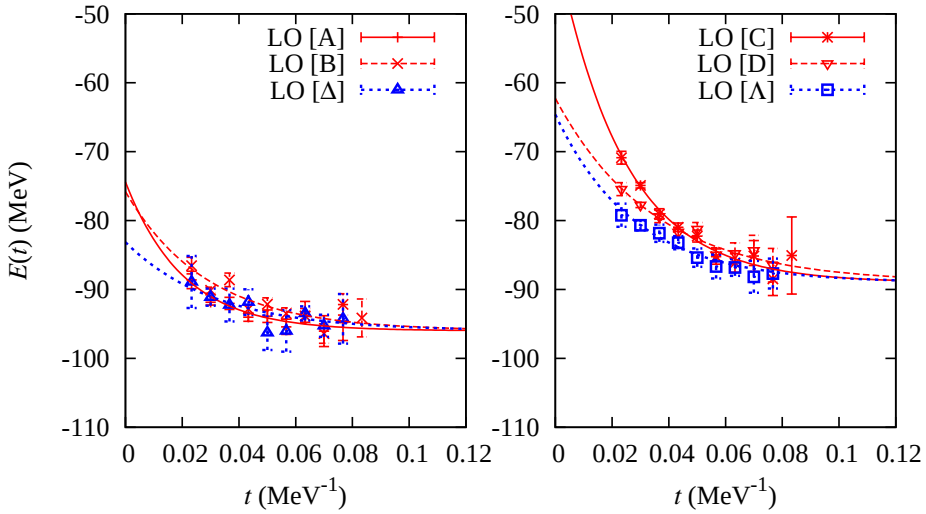

Figure 2: Results for the lowest 0^+ states in ^{12}C at LO. The left panel shows the results using various initial states, each of which approaches the ground state energy with increasing Euclidean time t. The right panel shows the results using other initial states. These trace out an intermediate plateau at an energy $\sim$7 MeV above the ground state.

handle on the systematic uncertainties inherent to the simulations. For more details, see, e. g., Ref. [17].

Using this framework, a number of interesting results has been obtained, such as the first *ab initio* calculation of the Hoyle state in ^{12}C [12,21], the study of the triple-alpha process under variations of some fundamental constants [23,24], the calculation of the ground state energies of the alpha-cluster nuclei up to ^{28}Si with an accuracy of about 1% [16], an *ab initio* calculation of the spectrum and structure of ^{16}O [25], and the first ever microscopic calculation of alpha-alpha scattering [26]. However, the employed NNLO action works well for alpha-type nuclei, but is less precise for other systems. Therefore, new forms of smearing including also the pion-exchange as well as a non-local distribution of lattice creation and annihilation operators have been employed to gain further insight. Based on these improved LO actions, it was found that nuclear physics is near a quantum phase transition from a Bose gas to the nuclear liquid, where the first alpha-cluster nuclei are formed [27]. Another important observation in that paper is related to the degree of locality of the contact interactions, that appears to play a major role when going to larger nuclei and nuclear or neutron matter, as recently emphasized in Ref. [28]. Furthermore, isotopic chains from H to O could be calculated and new insights into nuclear clustering was obtained recently, including also a new algorithm that for the first time allows to calculate density distributions in nuclei and the corresponding form factors [29]. Some selected topics from this rich spectrum of results will be discussed in what follows. Most of these results have been obtained on supercomputers like JUGENE and JUQUEEN at the Forschungszentrum Jülich. The CPU scaling is approximately quadratic in atomic number, so nuclei up to $A \simeq 40$ have been investigated. Going to larger nuclei requires more fine-tuned actions to suppress the remaining sign oscillations.

3.2 *Ab initio* calculation of alpha-alpha scattering

Let us now consider the α-α scattering as a prototypical nuclear reaction. This is related to the facts that processes involving α-type nuclei comprise a major part of stellar nucleosynthesis, and control the production of certain elements in stars. Also, *ab initio* calculations of scattering and reactions suffer from exponential or factorial scaling with the number of nucleons in the clusters, so therefore it was not possible so far to perform an *ab initio* calculation of α-α scattering. It is thus a challenging task to use the lattice to tackle such type of processes. We note that on the lattice one only has discrete energy levels, and therefore a direct calculation of scattering processes appears impossible. This hurdle can be overcome by the so-called adiabatic projection method, that splits the problem of the calculation of scattering and inelastic reactions into two parts. First, using the Euclidean time projection method, one constructs a low-energy cluster Hamiltonian, called the adiabatic Hamiltonian. In the second step, one then computes scattering phase shifts or reaction amplitudes using this adiabatic Hamiltonian. The method was developed and refined in Refs. [30–34] and resembles in the methodology the Hamiltonian matrix approach combining the no-core shell model with the resonating group method, see, e. g., Refs. [35–37]. In more detail, the construction of a low-energy effective theory for clusters proceeds as follows: One uses initial states as a direct product of two clusters located on the lattice, parameterized

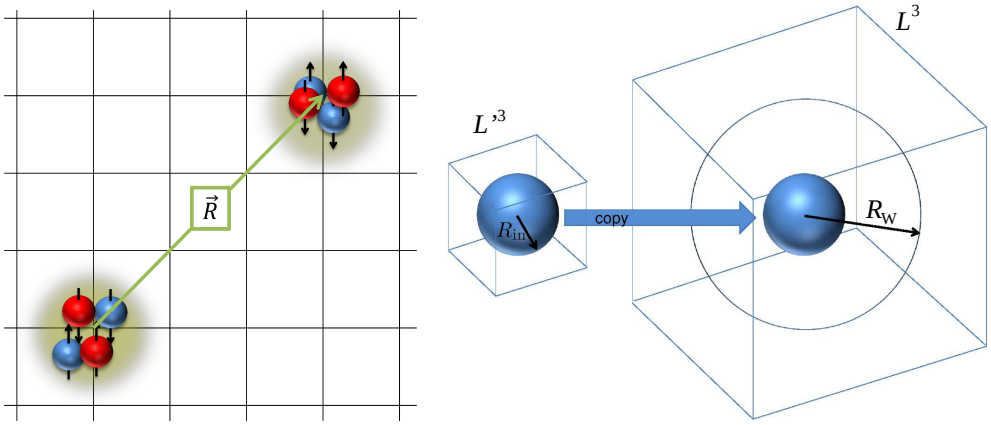

Figure 3: Left panel: A two-dimensional picture of the two-cluster initial state $|\vec{R}\rangle$ separated by the displacement vector $\vec{R}$. Right panel: A sketch of the lattices for the cluster-cluster calculations in the overlapping and in the noninteracting regions. $R_{\rm in}$ is the largest radial distance where the full adiabatic Hamiltonian is matched to the effective free cluster Hamiltonian without introducing any systematic errors. R_W indicates the radius of the spherical wall as discussed in the text.

by the relative separation between the clusters, as shown in the left panel of Fig. 3,

$$|\vec{R}\rangle = \sum_{\vec{r}} |\vec{r} + \vec{R}\rangle \otimes \vec{r}. \tag{6}$$

These are projected in Euclidean time with the chiral EFT Hamiltonian H, $|\vec{R}\rangle_\tau = \exp(-H\tau)|\vec{R}\rangle$. These so-called dressed cluster states include all possible interaction effects such as polarizations as well as deformations and, of course, the Pauli principle. The adiabatic Hamiltonian is then given by $[H_\tau]_{\vec{R}\vec{R}'} = {}_\tau\langle\vec{R}|H|\vec{R}'\rangle_\tau$. In general, this Hamiltonian needs to be normalized, which requires left and right multiplication with the corresponding norm matrices. What concerns the strong interactions, it can be shown that asymptotically, the adiabatic Hamiltonian is nothing but the free Hamiltonian for two clusters, eventually supplemented by infinite-range interactions as the Coulomb one. The underlying simulations can be simplified considerably by employing the so-called radial Hamiltonian based on the lattice version of angular momentum projection and binning the lattice points in rings of a given width. Further, the long-range Coulomb interaction can also be included exactly. For that, one performs first simulations in small box with a volume $L'^3 \sim (16\ \text{fm})^3$, with all interactions switched on. This is the supplemented by a second set of simulations in a large box with a volume of about $L^3 \sim (120\ \text{fm})^3$, where the strong interactions are turned off and the long-range Coulomb interaction is included by imposing Coulomb boundary conditions on a spherical wall with radius $R_W \simeq 40$ fm, see the right panel of Fig. 3. In that way, all effects of the strong and the electromagnetic interactions are included.

Using the same NNLO Hamiltonian as for the studies of the spectrum and structure of ^{12}C and ^{16}O, the S- and D-wave phase shifts have been computed in Ref. [26], as shown in Fig. 4. At LO in the employed counting, the Coulomb interaction is not included, so both the S- and D-wave phase shifts are off the data. This is visibly

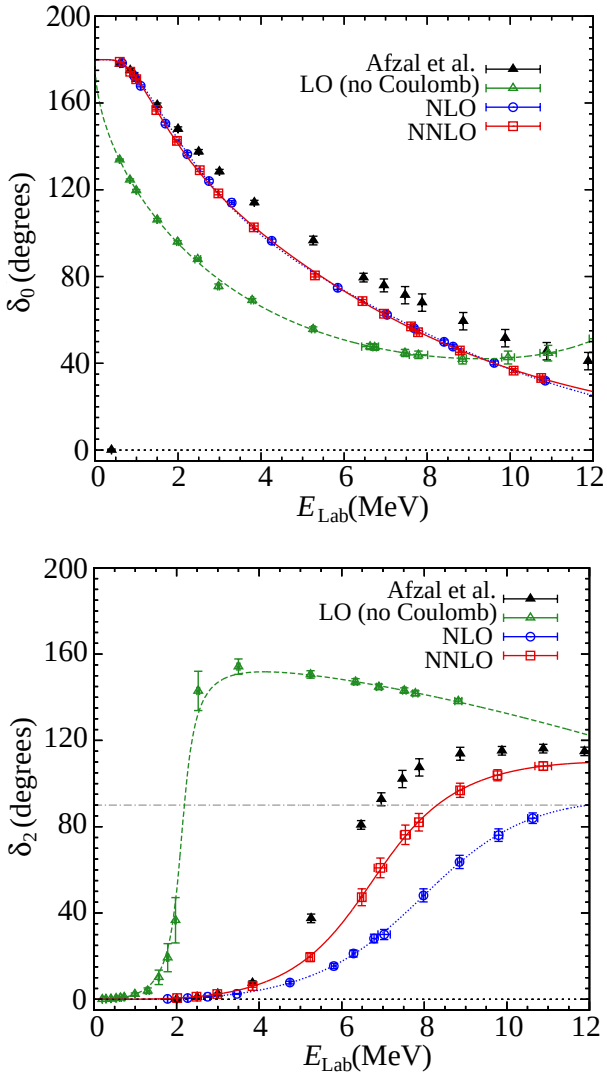

Figure 4: Upper panel: S-wave α-α phase shifts δ_0. Bottom panel: D-wave α-α phase shifts δ_2. Shown are the NLEFT LO (green triangles), NLO (blue circles) and NNLO (red squares) results. The data (black triangles with error bars) are from Ref. [38].

improved at NLO and further at NNLO for the D-wave. The small NNLO corrections in the S-wave are due to the coarse lattice spacing. Overall, one finds a good description of the scattering data. In the S-wave, we find a bound state corresponding to ^{8}Be that is bound by $-0.11(1)$ MeV, whereas in nature this nucleus is unbound by $+0.09$ MeV. This deviation of about 200 keV reflects the precision of the calculation. In the D-wave at NNLO, the resonance parameters are $E_R^{\rm NNLO} = 3.27(12)$ MeV and $\Gamma_R^{\rm NNLO} = 2.09(16)$ MeV, not far off the empirical data of 2.92(18) MeV and 1.35(50) MeV, respectively. Maybe the most significant result of this study is the fact that the computational time scales quadratically with the number of nucleons in the two clusters, $t_{\rm CPU} \sim (A_1 + A_2)^2$, with A_i being the number of nucleons in the cluster i ($i = 1, 2$). This means that the computational time for the so-called holy grail of nuclear astrophysics, the radiative alpha capture on ^{12}C at stellar energies (given by the Gamow peak), $\alpha + {}^{12}{\rm C} \to {}^{16}{\rm O} + \gamma$, is in reach, requiring only 8 times

as much CPU time as the computation of elastic α-α scattering (twice the number of nucleons and two channels). Before doing that, however, the chiral forces should be worked out to N3LO so as to reach the required accuracy.

3.3 New insights into nuclear clustering

Clustering in nuclei is an old but ever fascinating topic, introduced by Wheeler in 1937 in this seminal paper on "Molecular Viewpoints in Nuclear Structure" [39]. The most prominent type of clustering is the observation of α-particle substructures in light and medium-mass nuclei, and its eventual disappearance as the atomic number increases. There have been many works on alpha clustering, here I just mention recent work on alpha clustering employing density functional methods by the Peking group [40] as well as work by the Paris–Zagreb group [41]. For a recent review, see, e. g., Ref. [42].

As already mentioned above, alpha clustering emerges naturally in NLEFT and a number of intriguing results on alpha-type nuclei and clustering have already been obtained, such as the first *ab initio* calculation of the Hoyle state or the observation that nuclear physics is close to a quantum phase transition from a Bose gas of α's to a nuclear liquid for α-type nuclei. However, when adding extra neutrons and/or protons, the precision of the calculations quickly deteriorates due to the remaining sign oscillations. To overcome this, a new LO action with smeared SU(4) local and non-local symmetric contact interactions as well as smeared one-pion exchange was constructed in Ref. [29]. The non-local smearing distributes any nucleon creation and/or annihilation operator over the six neighboring lattice sites as depicted in the left panel of Fig. 5,

$$a_{\rm NL}^{(\dagger)}(\mathbf{n}) = a^{(\dagger)}(\mathbf{n}) + s_{\rm NL} \sum_{\langle \mathbf{n}' \, \mathbf{n} \rangle} a^{(\dagger)}(\mathbf{n}'), \tag{7}$$

where $s_{\rm NL}$ is a real parameter, and the notation $\sum_{\langle \mathbf{n}' \, \mathbf{n} \rangle}$ represents the summation over nearest-neighbor lattice sites of the site $\mathbf{n}$. While this smearing was originally designed to just suppress the remaining sign oscillations when extra neutrons and/or protons are added to alpha-type nuclei, it turned out to work much better. For that, consider a LO action that is SU(4) symmetric with local and non-local smearing as well as smeared one-pion exchange. This action has three LECs, the strength of the SU(4)-symmetric contact term, the parameter related to the degree of locality of the interaction and the above-mentioned $s_{\rm NL}$. Fitting these to the average np S-wave scattering lengths and effective ranges and also to the α-α S-wave scattering length, one can predict the isotope chains from hydrogen to oxygen as shown in the right panel of Fig. 5. These have an accuracy of 0.7 MeV per nucleon or better. This is quite amazing given this highly simplified LO action. Clearly, NLO effects (and higher orders) need to be accounted for to achieve, e. g., a better description of the ${}^1S_0$ np phase.

Using this action, one can also obtain deeper insight into nuclear clustering. For that, define as probes of alpha clusters the quantities

$$\rho_4 = \sum_{\mathbf{n}} : \rho^4(\mathbf{n})/4! : \quad \text{and} \quad \rho_3 = \sum_{\mathbf{n}} : \rho^3(\mathbf{n})/3! : . \tag{8}$$

Here, ρ_4 couples to the center of the α-cluster while ρ_3 gets contributions from a wider portion of the alpha-particle wave function and thus these can be used for "measuring" cluster properties. Note that ρ_3 and ρ_4 depend on the regulator, the

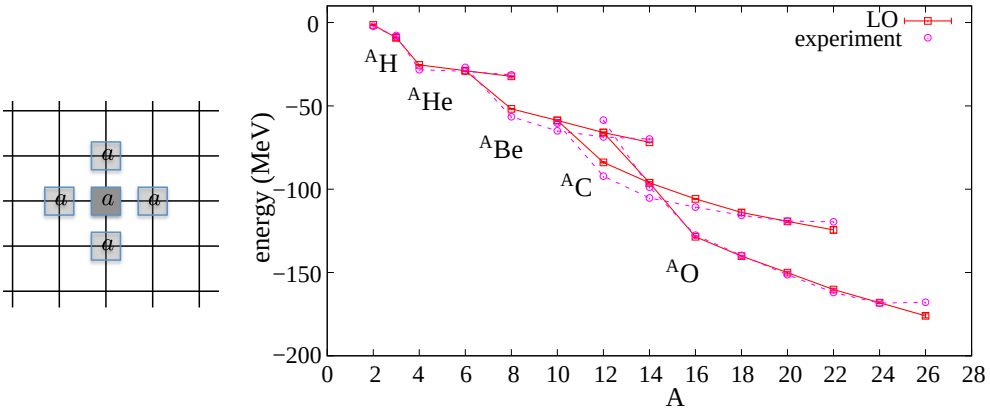

Figure 5: Left panel: Two-dimensional illustration of the non-local smearing of a nucleon creation/annihilation operator over the neighboring lattice sites. Right panel: The ground state energies versus the number of nucleons A for the hydrogen, helium, beryllium, carbon, and oxygen isotopes (NLEFT: squares with error bars, experiment: circles). The errors are one-standard deviation error bars associated with the stochastic errors and the extrapolation to an infinite number of time steps.

lattice spacing a, but not on the nucleus. However, the ratios $\rho_3/\rho_{3,\alpha}$ and $\rho_4/\rho_{4,\alpha}$ are free from short-distance ambiguities. If properly defined, the effective number of alpha clusters should be greater than or equal to N_α. A value equal to N_α indicates that the alpha clusters are behaving as indivisible objects, and the nucleus can be regarded as a compound fluid of alpha particles and neutrons. If the effective number is significantly greater than N_α, then the description in terms of individual alpha clusters breaks down and the system behaves more as a nuclear liquid of protons and neutrons. The behavior is shown in the left panel of Fig. 6, where it is seen that, for the oxygen isotope chain, the entanglement between the clusters leads to the expectation values of $\rho_3/\rho_{3,\alpha}$ and $\rho_4/\rho_{4,\alpha}$ much larger than 4. This shows that the transition from cluster-like states in light systems to nuclear liquid-like states in heavier systems should not be viewed as a simple suppression of multi-nucleon short-distance correlations, but rather as an increasing *entanglement* of the nucleons involved in the multi-nucleon correlations.

Another important development of Ref. [29] was the formulation of the so-called pinhole algorithm, see the right panel of Fig. 6. In general, auxiliary field quantum MC calculations involve states that are superpositions of many different center-of-mass (cm) positions, so a direct calculation of density distributions of nucleons in a nucleus is not possible. This can be overcome by inserting a screen with pinholes with spin and isospin labels that allows nucleons with corresponding spin and isospin to pass. In that way, one measures the A-body density operator

$$\rho_{i_1,j_1,\ldots,i_A,j_A}(\mathbf{n}_1,\ldots,\mathbf{n}_A) = :\rho_{i_1,j_1}(\mathbf{n}_1)\ldots\rho_{i_A,j_A}(\mathbf{n}_A): \,. \tag{9}$$

MC sampling of the amplitude

$$A_{i_1,j_1,\ldots,i_A,j_A}(\mathbf{n}_1,\ldots,\mathbf{n}_A,L_t) = \langle\psi(\tau/2)|\rho_{i_1,j_1,\ldots,i_A,j_A}(\mathbf{n}_1,\ldots,\mathbf{n}_A)|\psi(\tau/2)\rangle \tag{10}$$

then allows to measure the proton and neutron densities as well as more complicated

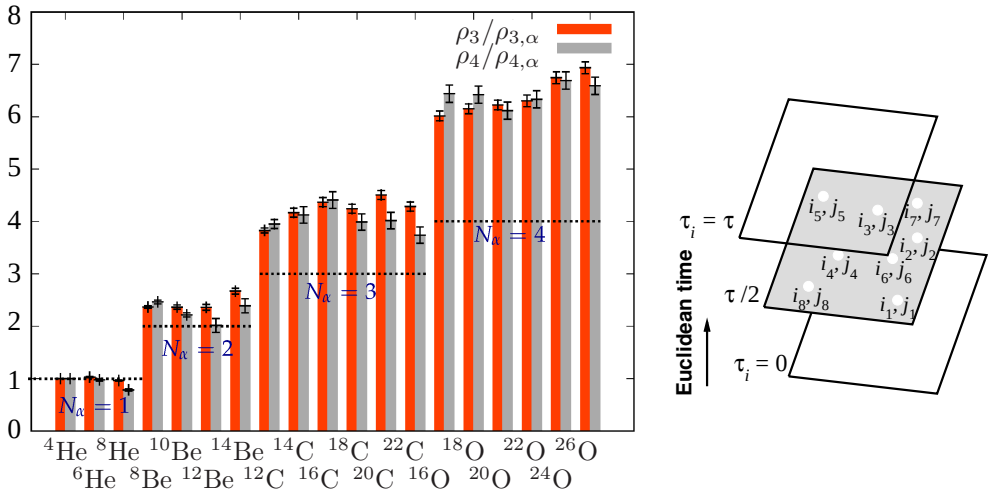

Figure 6: Left panel: The ratios $\rho_3/\rho_{3,\alpha}$ and $\rho_4/\rho_{4,\alpha}$ for the helium, beryllium, carbon and oxygen isotopes. For orientation, we also indicate by the dashed lines the expected number of α-clusters, N_α. Right panel: Sketch of the pinhole locations and spin-isospin indices at time $t = L_t a_t/2$.

two-, three- or higher-body correlations of nucleons within a given nucleus. This is because the pinhole sheet allows one to determine the cm of a given nucleus given simply by the minimal distance to all nucleons. Further, the resolution of this method is a/A because the cm position $\mathbf{r}_{\rm cm}$ is an integer $\mathbf{n}_{\rm cm}$ times a/A. Results for the proton and neutron distributions in the isotopes ^{12,14,16}C are shown in the upper panel of Fig. 7. The proton size of $r_E^p = 0.84\,\text{fm}$ [43, 44] is accounted for and asymptotic properties for the volume dependence of N-body bound states [45] have been used. Upon the Fourier-transformation of these densities, one can obtain the corresponding elastic form factor. This is shown in the bottom panel of Fig. 7 for ^{12}C. Given the simplicity of the underlying Hamiltonian, the agreement is quite satisfactory. This paves the way for detailed nuclear structure studies.

3.4 Fine-tunings and the multiverse

In nuclear physics, we observe a number of so-called fine-tunings, for some reviews and recent works, see, e. g., Refs. [47–51]. A prominent example is the lightest nucleus, the deuteron. It is bound by a mere 2 MeV, just one tenth of percent of its total mass. Also, the aforementioned Hoyle state must be very closely placed to the triple-alpha threshold, in nature the energy difference is just 380 keV, much less than typical nuclear excitation energies of a few MeV. This close proximity is required so that in hot, old stars a sufficient amount of carbon and also oxygen is generated [22]. It is therefore natural to ask how much the SM fundamental parameters can be detuned so that this resonance condition is no longer viable? First, however, we must find out what the relevant parameters are. Nuclear binding is a delicate balance between the attractive strong and the repulsive electromagnetic interactions. The latter are given in terms of Sommerfeld's fine-structure constant, $\alpha_{\rm EM} \simeq 1/137$. As concerns the strong interaction, the strong coupling constant α_S is intimately tied to

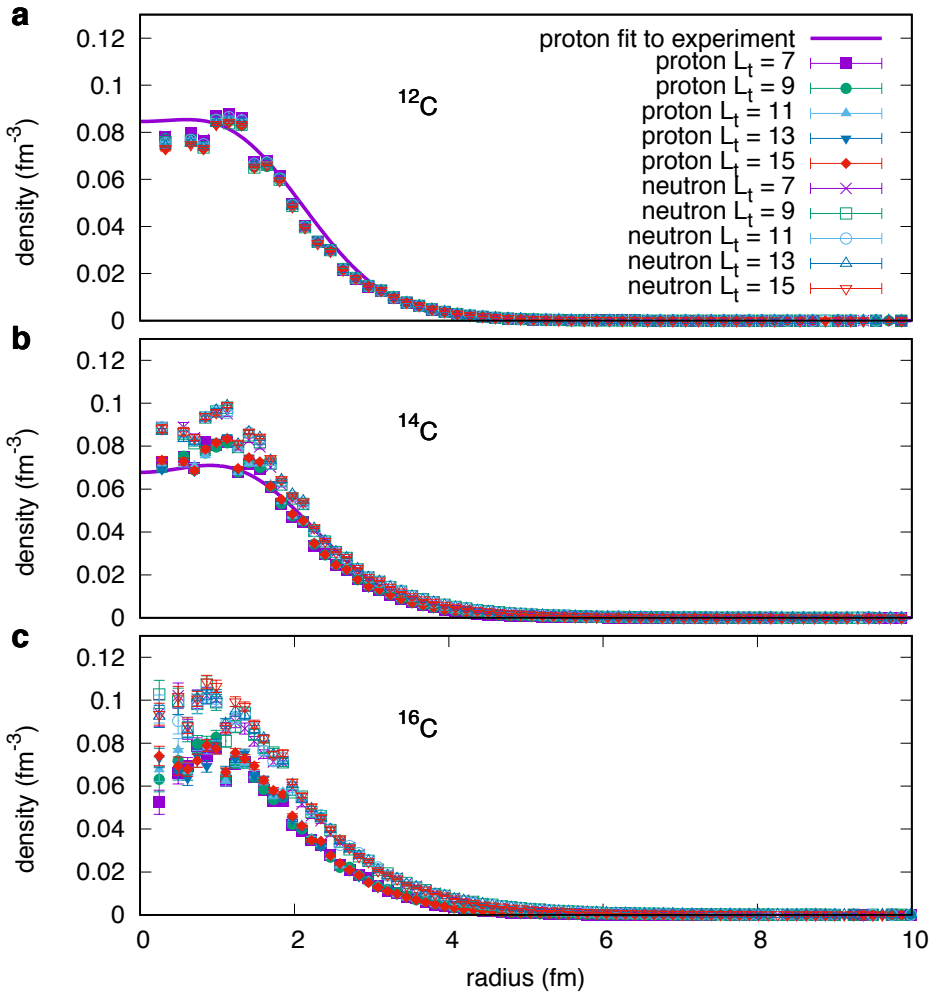

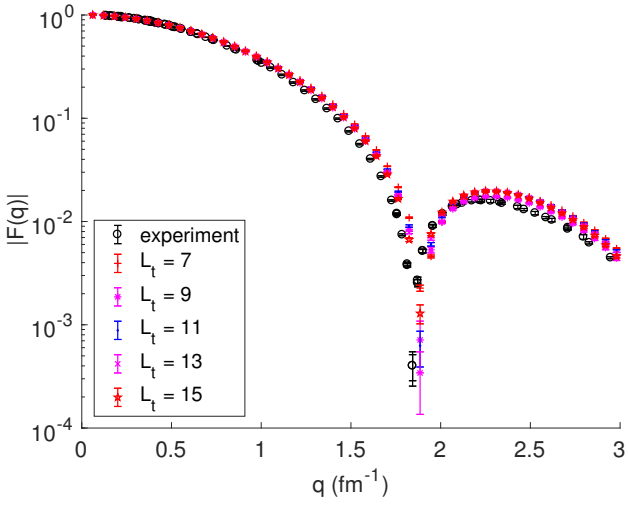

Figure 7: Upper panel: Proton and neutron densities for the ground states of ^{12,14,16}C versus radial distance for the MC data with $L_t = 9, 11, 13, 15$ time steps. The experimental data are from Ref. [46]. Bottom panel: Elastic form factor of ^{12}C. Data: black open symbols.

the nucleon mass because of dimensional transmutation, and therefore the small light quark masses m_u, m_d are the relevant parameters that control nuclear binding. This appears at first counter-intuitive, as the major part of the nucleon mass is given by gluon field energy by means of the trace anomaly, while the light quark contribution to the nucleon mass is given by the so-called pion-nucleon σ-term, $\sigma_{\pi N} = 59(3)\,\mathrm{MeV}$ [52]. However, the quark mass values of a few MeV (which are, of course, scale- and scheme-dependent) are of the same size as the nuclear binding energy per nucleon, E/A, so that these are the pertinent strong interaction parameters. To be more precise, the rate of the triple-alpha process is given by $r_{3\alpha} \sim \Gamma_\gamma \exp\left(-\Delta E/kT\right)$, with k being the Boltzmann constant, T is the temperature, Γ_γ is the width of the Hoyle state and $\Delta E = E_{12}^\star - 3E_\alpha = 379.47(18)$ keV, where $E^\star$ is the energy of the Hoyle state. The question now is how much can the ΔE be changed so that there is still enough ^{12}C and ^{16}O produced in the stars? This was answered in a calculation of the element generation in stars by varying ΔE but no other parameter. It turned out that the allowed variation is $\delta|\Delta E| \lesssim 100$ keV [53, 54], which does not appear to be any form of fine-tuning. Note that very recent stellar simulations appear to soften this envelope [55]. However, one still has to make the connection to the fundamental parameters of the SM. While this can be done for the electromagnetic interactions in cluster-type models as used, e. g., in Ref. [53], the variation of the quark masses requires a more microscopic framework as provided by chiral EFT. This is depicted for the quark mass dependence of the LO NN force in the upper panel of Fig. 8. Here, the quark mass and pion mass dependences can be used synonymously, as the Gell-Mann–Oakes–Renner relation, $M_\pi^2 \sim m_u + m_d$, is fulfilled to better than 94% in QCD [56]. As can be seen from this figure, there are explicit (through the pion propagator) and implicit (through the pion-nucleon coupling, the nucleon mass and the four-nucleon couplings) pion mass dependences. All this can be accounted for systematically and precisely using chiral EFT. Coming back to the triple alpha-process, nuclear lattice simulations are the appropriate tool to study its dependence on the fundamental parameters, for details see Refs. [23, 24]. For that, one has to translate the condition $\delta|\Delta E| \lesssim 100$ keV into a constraint for the quark masses (and similarly for the fine-structure constant). For the quark masses, it reads (for fixed α_{EM})

$$\left|\Big(0.571(14)\bar{A}_s + 0.934(11)\bar{A}_t - 0.069(6)\Big)\frac{\delta m_q}{m_q}\right| < 0.0015, \tag{11}$$

with the average light quark mass (as the strong isospin breaking plays no role here) $m_q = (m_u + m_d)/2$, $\bar{A}_{s,t} \equiv \partial a_{s,t}^{-1}/\partial M_\pi\big|_{M_\pi^{\mathrm{phys}}}$, where a_s and a_t denote the singlet and the triplet NN scattering length, respectively. Independently of the precise values of these two quantities, it can be shown that the various fine-tunings in the triple-alpha process (the closeness of the ^{8}Be binding energy to the 2α threshold and the closeness of the Hoyle state to the 3α threshold) are indeed correlated. This had been speculated before [58] but could only be worked out precisely using NLEFT. Bounds on $\bar{A}_{s,t}$ had been obtained earlier based on resonance saturation of $4N$ operators [59] in Ref. [57] (see also Ref. [60]) as shown by the black cross in the bottom panel of Fig. 8. The fairly large uncertainty can eventually be overcome using lattice QCD to calculate these quantities. In the plane of $\bar{A}_s$-$\bar{A}_t$, varying the quark mass leads to diagonal bands whose widths depends on the assumed variations. This is shown for variations of $\delta m_q/m_q$ of 0.5, 1 and 5% by the three different bands. Clearly, a smaller

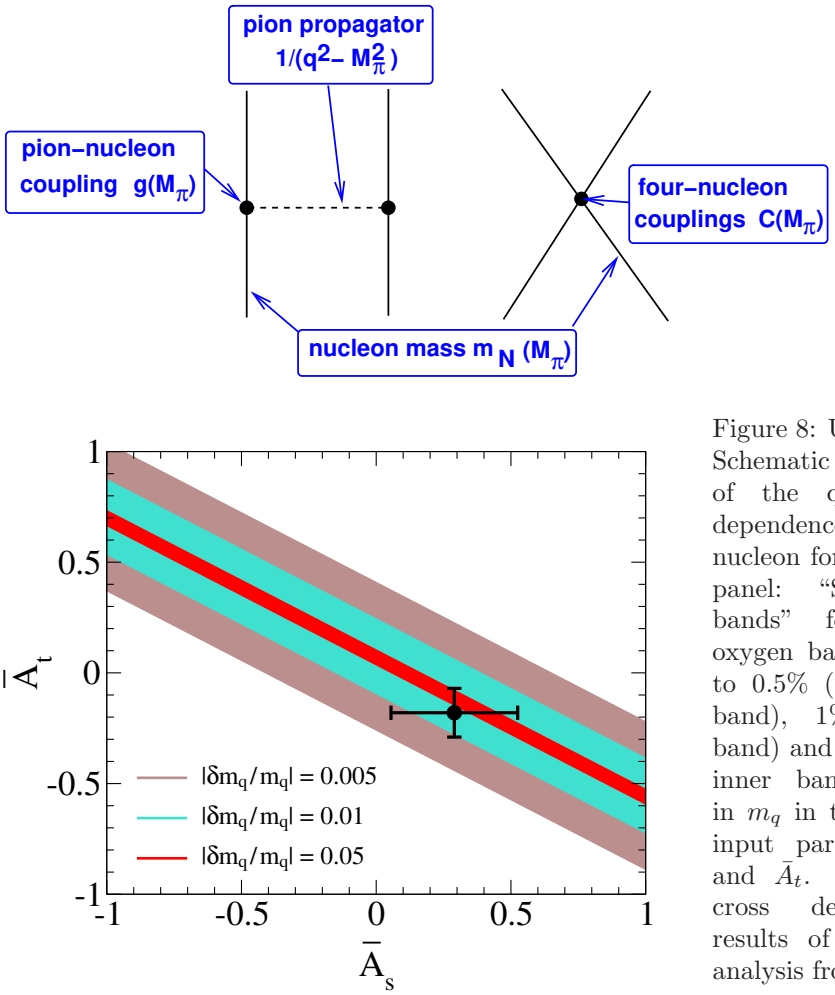

Figure 8: Upper panel: Schematic drawing of the quark mass dependence in the two-nucleon force. Bottom panel: "Survivability bands" for carbon-oxygen based life due to 0.5% (broad outer band), 1% (medium band) and 5% (narrow inner band) changes in m_q in terms of the input parameters $\bar{A}_s$ and $\bar{A}_t$. The black cross denotes the results of the N2LO analysis from [57].

variation leads to a broader band. If one focuses on the central value of $\bar{A}_{s,t}$, one finds that the m_q variations of 2−3% are allowed so that the abovementioned condition is fulfilled. The large uncertainties in $\bar{A}_{s,t}$ do not allow for a more precise statement. For $\alpha_{\rm EM}$, no such uncertainties are present and it can be stated with certainty that it can be varied by at most 2.5%. Also, no other bounds are found if one varies both the quark masses and the fine-structure constant at the same time. This is clearly a stronger fine-tuning as for $|\Delta E|$ and its consequences for our anthropic view of the Universe are discussed in Ref. [61]. Lattice QCD can be used to tighten the bounds on $\bar{A}_{s,t}$, for the state-of-the-art see Ref. [62].

4 Summary and outlook

Let me briefly summarize the main messages of this talk:

- Chiral EFT for nuclear forces provides a precise framework for $2N$ and $3N$

forces with small uncertainties, as discussed by Evgeny Epelbaum [1] in these Proceedings. The nuclear forces from chiral EFT can also be formulated for varying strong and electromagnetic forces, which is a necessary requirement to study various fine-tunings in nuclear physics.

- Nuclear lattice simulations are a new quantum many-body approach that is based on the successful continuum nuclear chiral EFT. Already a number of intriguing results have been obtained based on NLEFT. In particular, the clustering emerges naturally and α-cluster nuclei are well described. Further, with an improved chiral action based on non-local smearing, neutron- and proton-rich nuclei can also be studied. With the invention of the pinhole algorithm, the calculation of charge densities and form factors has become possible. Furthermore, a fine-tuning in nuclear reactions can be studied.

- Various bridges to the lattice QCD studies need to be explored, in particular, in pinning down some of the LECs related to multi-nucleon forces or the quark mass dependence of multi-nucleon operators.

- Finally, it must be said that many open issues in nuclear structure and reaction physics can now be addressed in a truly quantitative manner. For example, the "holy grail" of nuclear astrophysics [63], the *ab initio calculation* of the reaction $^4\mathrm{He} + {}^{12}\mathrm{C} \to {}^{16}\mathrm{O} + \gamma$, is in reach.

More recent developments in NLEFT will be covered in Dean Lee's contribution [4].

Acknowledgements

I thank the organizers for giving me an opportunity to present these thoughts at this interesting workshop. I am grateful to all my collaborators, who have contributed to my understanding of the issues discussed here. Partial financial support by the CAS (2018DM0034), DFG (TRR 110), and VolkswagenStiftung (grant no. 93562) is gratefully acknowledged.

References

[1] E. Epelbaum, *see these Proceedings*, p. 150, http://www.ntse.khb.ru/files/uploads/2018/proceedings/Epelbaum.pdf.

[2] S. Weinberg, Phys. Lett. B **251**, 288 (1990).

[3] S. Weinberg, Nucl. Phys. B **363**, 3 (1991).

[4] D. Lee, *see these Proceedings*, p. 45, http://www.ntse.khb.ru/files/uploads/2018/proceedings/Lee.pdf.

[5] E. Epelbaum, H.-W. Hammer and U.-G. Meißner, Rev. Mod. Phys. **81**, 1773 (2009).

[6] B. Borasoy, E. Epelbaum, H. Krebs, D. Lee and U.-G. Meißner, Eur. Phys. J. A **31**, 105 (2007).

[7] E. Epelbaum, H. Krebs, D. Lee and U.-G. Meißner, Eur. Phys. J. A **45**, 335 (2010).

[8] E. Wigner, Phys. Rev. **51**, 106 (1937).

[9] J. W. Chen, D. Lee and T. Schäfer, Phys. Rev. Lett. **93**, 242302 (2004).

[10] D. Lee, Prog. Part. Nucl. Phys. **63**, 117 (2009).

[11] T. A. Lähde and U.-G. Meißner, *Nuclear lattice effective field theory: An introduction*. Springer-Verlag, Heidelberg (*in print*).

[12] E. Epelbaum, H. Krebs, D. Lee and U.-G. Meißner, Phys. Rev. Lett. **106**, 192501 (2011).

[13] B. Borasoy, E. Epelbaum, H. Krebs, D. Lee and U.-G. Meißner, Eur. Phys. J. A **35**, 343 (2008).

[14] B. N. Lu, T. A. Lähde, D. Lee and U.-G. Meißner, Phys. Lett. B **760**, 309 (2016).

[15] E. Epelbaum, H. Krebs, D. Lee and U.-G. Meißner, Phys. Rev. Lett. **104**, 142501 (2010).

[16] T. A. Lähde, E. Epelbaum, H. Krebs, D. Lee, U.-G. Meißner and G. Rupak, Phys. Lett. B **732**, 110 (2014).

[17] T. A. Lähde *et al.*, J. Phys. G **42**, 034012 (2015).

[18] J. M. Alarcon *et al.*, Eur. Phys. J. A **53**, 83 (2017).

[19] N. Klein, S. Elhatisari, T. A. Lähde, D. Lee and U.-G. Meißner, Eur. Phys. J. A **54**, 121 (2018).

[20] N. Li, S. Elhatisari, E. Epelbaum, D. Lee, B. N. Lu and U.-G. Meißner, Phys. Rev. C **98**, 044002 (2018).

[21] E. Epelbaum, H. Krebs, T. A. Lähde, D. Lee and U.-G. Meißner, Phys. Rev. Lett. **109**, 252501 (2012).

[22] F. Hoyle, Astrophys. J. Suppl. **1**, 121 (1954).

[23] E. Epelbaum, H. Krebs, T. A. Lähde, D. Lee and U.-G. Meißner, Phys. Rev. Lett. **110**, 112502 (2013).

[24] E. Epelbaum, H. Krebs, T. A. Lähde, D. Lee and U.-G. Meißner, Eur. Phys. J. A **49**, 82 (2013).

[25] E. Epelbaum *et al.*, Phys. Rev. Lett. **112**, 102501 (2014).

[26] S. Elhatisari *et al.*, Nature **528**, 111 (2015).

[27] S. Elhatisari *et al.*, Phys. Rev. Lett. **117**, 132501 (2016).

[28] B. N. Lu, N. Li, S. Elhatisari, D. Lee, E. Epelbaum and U.-G. Meißner, arXiv:1812.10928 [nucl-th] (2018).

[29] S. Elhatisari *et al.*, Phys. Rev. Lett. **119**, 222505 (2017).

[30] G. Rupak and D. Lee, Phys. Rev. Lett. **111**, 032502 (2013).

[31] M. Pine, D. Lee and G. Rupak, Eur. Phys. J. A **49**, 151 (2013).

[32] S. Elhatisari and D. Lee, Phys. Rev. C **90**, 064001 (2014).

[33] A. Rokash, M. Pine, S. Elhatisari, D. Lee, E. Epelbaum and H. Krebs, Phys. Rev. C **92**, 054612 (2015).

[34] S. Elhatisari, D. Lee, U. G. Meißner and G. Rupak, Eur. Phys. J. A **52**, 174 (2016).

[35] P. Navrátil and S. Quaglioni, Phys. Rev. C **83**, 044609 (2011).

[36] P. Navrátil, R. Roth and S. Quaglioni, Phys. Lett. B **704**, 379 (2011).

[37] P. Navrátil and S. Quaglioni, Phys. Rev. Lett. **108**, 042503 (2012).

[38] S. A. Afzal, A. A. Z. Ahmad and S. Ali, Rev. Mod. Phys. **41**, 247 (1969).

[39] J. A. Wheeler, Phys. Rev. **52**, 1083 (1937).

[40] P. W. Zhao, N. Itagaki and J. Meng, Phys. Rev. Lett. **115**, 022501 (2015).

[41] J.-P. Ebran, E. Khan, T. Niksic and D. Vretenar, Nature **487**, 341 (2012).

[42] M. Freer, H. Horiuchi, Y. Kanada-En'yo, D. Lee and U. G. Meißner, Rev. Mod. Phys. **90**, 035004 (2018).

[43] M. A. Belushkin, H.-W. Hammer and U.-G. Meißner, Phys. Rev. C **75**, 035202 (2007).

[44] R. Pohl *et al.*, Nature **466**, 213 (2010).

[45] S. König and D. Lee, Phys. Lett. B **779**, 9 (2018).

[46] F. J. Kline, H. Crannell, J. T. O' Brien, J. Mccarthy and R. R. Whitney, Nucl. Phys. A **209**, 381 (1973).

[47] C. J. Hogan, Rev. Mod. Phys. **72**, 1149 (2000).

[48] R. L. Jaffe, A. Jenkins and I. Kimchi, Phys. Rev. D **79**, 065014 (2009).

[49] L. A. Barnes, Publ. Astron. Soc. Austral. **29**, 529 (2012).

[50] A. N. Schellekens, Rev. Mod. Phys. **85**, 1491 (2013).

[51] J. F. Donoghue, Annu. Rev. Nucl. Part. Sci. **66**, 1 (2016).

[52] M. Hoferichter, J. Ruiz de Elvira, B. Kubis and U.-G. Meißner, Phys. Rev. Lett. **115**, 092301 (2015).

[53] H. Oberhummer, A. Csoto and H. Schlattl, Science **289**, 88 (2000).

[54] H. Schlattl, A. Heger, H. Oberhummer, T. Rauscher and A. Csoto, Astrophys. Space Sci. **291**, 27 (2004).

[55] L. Huang, F. C. Adams and E. Grohs, Astropart. Phys. **105**, 13 (2019).

[56] G. Colangelo, J. Gasser and H. Leutwyler, Phys. Rev. Lett. **86**, 5008 (2001).

[57] J. C. Berengut *et al.*, Phys. Rev. D **87**, 085018 (2013).

[58] S. Weinberg, *Facing up*. Harvard University Press, Cambridge, MA, 2001.

[59] E. Epelbaum, U.-G. Meißner, W. Gloeckle and C. Elster, Phys. Rev. C **65**, 044001 (2002).

[60] P. F. Bedaque, T. Luu and L. Platter, Phys. Rev. **C83**, 045803 (2011).

[61] U.-G. Meißner, Sci. Bull. **60**, 43 (2015).

[62] V. Baru, E. Epelbaum and A. A. Filin, Phys. Rev. C **94**, 014001 (2016).

[63] W. A. Fowler, Rev. Mod. Phys. **56**, 149 (1984).